

RADC-TR-80-300
In-House Report
September 1980

76
LEVEL 4
W



AD A 098 939

ELECTROMAGNETIC WAVE SCATTERING FROM ROUGH TERRAIN

Robert J. Papa
John F. Lennon
Richard L. Taylor

APPROVED FOR PUBLIC RELEASE; DISTRIBUTION UNLIMITED

DTIC
ELECTE
MAY 15 1981

A

ROME AIR DEVELOPMENT CENTER
Air Force Systems Command
Griffiss Air Force Base, New York 13441

FILE COPY

81 5 15 053

This report has been reviewed by the RADC Public Affairs Office (PA) and is releasable to the National Technical Information Service (NTIS). At NTIS it will be releasable to the general public, including foreign nations.

RADC-TR-80-300 has been reviewed and is approved for publication.

APPROVED:

John K. Schindler

JOHN K. SCHINDLER
Assistant Branch Chief
EM Techniques Branch
Electromagnetic Sciences Division

APPROVED:

Allan C. Schell

ALLAN C. SCHELL, Chief
Electromagnetic Sciences Division

FOR THE COMMANDER:

John P. Huss

JOHN P. HUSS
Acting Chief, Plans Office

SUBJECT TO EXPORT CONTROL LAWS

This document contains information for manufacturing or using munitions of war. Export of the information contained herein, or release to foreign nationals within the United States, without first obtaining an export license, is a violation of the International Traffic in Arms Regulations. Such violation is subject to a penalty of up to 2 years imprisonment and a fine of \$100,000 under 22 U.S.C 2778.

Include this notice with any reproduced portion of this document.

If your address has changed or if you wish to be removed from the RADC mailing list, or if the addressee is no longer employed by your organization, please notify RADC (EECT) Hanscom AFB MA 01731. This will assist us in maintaining a current mailing list.

Do not return this copy. Retain or destroy.

Unclassified

SECURITY CLASSIFICATION OF THIS PAGE (When Data Entered)

REPORT DOCUMENTATION PAGE		READ INSTRUCTIONS BEFORE COMPLETING FORM
1. REPORT NUMBER RADC-TR-88-399 ✓	2. GOVT ACCESSION NO. AD-A098939	3. RECIPIENT'S CATALOG NUMBER
4. TITLE (and Subtitle) ELECTROMAGNETIC WAVE SCATTERING FROM ROUGH TERRAIN		5. TYPE OF REPORT & PERIOD COVERED In-house
6. AUTHOR(s) Robert J. Papa John F. Lennon Richard L. Taylor		7. PERFORMING ORG. REPORT NUMBER
8. PERFORMING ORGANIZATION NAME AND ADDRESS Deputy for Electronic Technology (RADC/EEC) Hanscom AFB Massachusetts 01731		9. CONTRACT OR GRANT NUMBER(s) 12 39
10. CONTROLLING OFFICE NAME AND ADDRESS Deputy for Electronic Technology (RADC/EEC) Hanscom AFB Massachusetts 01731		11. PROGRAM ELEMENT, PROJECT, TASK AREA & WORK UNIT NUMBERS
12. MONITORING AGENCY NAME & ADDRESS (if different from Controlling Office)		13. REPORT DATE 12 September 1980
		14. NUMBER OF PAGES 38
		15. SECURITY CLASS (of this report) Unclassified
		16. DECLASSIFICATION/DOWNGRADING SCHEDULE
17. DISTRIBUTION STATEMENT (of this Report) Recommended for public release; distribution unlimited.		
18. DISTRIBUTION STATEMENT (of abstract entered in Block 20, if different from Report)		
19. SUPPLEMENTARY NOTES		
20. KEY WORDS (Continue on reverse side if necessary and identify by block number) Terrain characterization Statistical analysis Rough-surface scattering Electromagnetics		
21. ABSTRACT (Continue on reverse side if necessary and identify by block number) This report presents two aspects of a program designed to calculate electromagnetic scattering from rough terrain: (1) the use of statistical estimation techniques to determine topographic parameters and (2) the results of a single-roughness-scale scattering calculation based on those parameters, including comparison with experimental data. In the statistical part of the present calculation, digitized topographic maps are used to generate data bases for the required scattering cells. The application of estimation theory to the data leads to the specification of		

DD FORM 1 JAN 79 1473

Unclassified

SECURITY CLASSIFICATION OF THIS PAGE (When Data Entered)

next page

200050

JOS

Unclassified

SECURITY CLASSIFICATION OF THIS PAGE(When Data Entered)

20. (Cont)

cont. → statistical parameters for each cell. The estimated parameters are then used in a hypothesis test to decide on a probability density function (PDF) that represents the height distribution in the cell. Initially, the formulation uses a single observation of the multivariate data. A subsequent approach involves multiple observations of the heights on a bivariate basis, and further refinements are being considered.

The electromagnetic scattering analysis, the second topic, calculates the amount of specular and diffuse multipath power reaching a monopulse receiver from a pulsed beacon positioned over a rough earth. The program allows for spatial inhomogeneities and multiple specular reflection points. The analysis of shadowing by the rough surface has been extended to the case where the surface heights are distributed exponentially. The calculated loss of bore-sight pointing accuracy attributable to diffuse multipath is then compared with the experimental results. The extent of the specular region, the use of localized height variations, and the effect of the azimuthal variation in power pattern are all assessed.

↖

Unclassified

SECURITY CLASSIFICATION OF THIS PAGE(When Data Entered)

Preface

The authors gratefully acknowledge the contributions of Dr. John K. Schindler RADC/EEC and Dr. Peter R. Franchi RADC/EEA, whose comments, suggestions, and constructive criticism have proved invaluable.

Accession For	
GRA&I	<input checked="" type="checkbox"/>
TAB	<input type="checkbox"/>
Announced	<input type="checkbox"/>
Classification	
Distribution/	
Availability Codes	
Avail and/or	
Special	
MS	A

Contents

1. INTRODUCTION	7
2. STATISTICAL ANALYSIS	10
2.1 Single Observation Formulation	10
2.2 Multiple Observation Formulation	13
3. SITE CHARACTERIZATION	16
4. ELECTROMAGNETIC SCATTERING ANALYSIS	17
4.1 Scattering Cross Section	18
4.2 Shadowing	20
4.3 Program Initiation	20
4.4 Specular Multipath	21
4.5 The Glistening Surface	21
4.6 Diffuse Multipath	22
4.7 Boresight Error	23
5. RESULTS AND CONCLUSIONS	24
5.1 Experimental Conditions	24
5.2 Coherent Power Results	25
5.3 Boresight Error Results	28
5.4 Diffuse Multipath Power	31
5.5 Conclusion	31
REFERENCES	32
APPENDIX A: The Shadowing Function for Exponentially Distributed Surface Heights	33
APPENDIX B: Specular Region Characterization	35
APPENDIX C: The Azimuthal Variation of the Monopulse Difference Pattern	37

Illustrations

1. Boxes Along Trajectory Which Contribute to Specular and Diffuse Multipath	10
2. Reflection of Radar Waves From Rough Terrain	21
3. Fresnel Zone Dimensions	22
4. The Glistening Surface	22
5. Experimental Data: Sum Signal (P_{coh}) vs Range	26
6. Experimental Data: Azimuthal Error (σ_θ) vs Range	26
7. Theoretical Calculations and Experimental Data: Sum Signal vs Range	27
8. Theoretical Calculations and Experimental Data: Sum Signal vs Range (system losses = -5 dB)	28
9. Theoretical Calculations: σ_θ vs Range, $k_m = 1.5$, Shadowing, Exponential PDF	29
10. Theoretical Calculations: σ_θ vs Range, $k_m = 1.7$, Shadowing Exponential PDF	29
11. Theoretical Calculations: σ_θ vs Range, $k_m = 1.5$, Shadowing, Normal PDF	30
12. Theoretical Calculations: σ_θ vs Range, $k_m = 1.5$, Shadowing, Exponential PDF, Azimuthal Pattern Variations	31
13. Theoretical Calculations: Diffuse Power (PDIFF) vs Range, $k_m = 1.5$, Shadowing, Exponential PDF, Azimuthal Pattern Variation	31
C1. Monopulse Difference Pattern in Azimuthal Plane	39

Tables

1. Experimental Conditions for DABS Tests	25
---	----

Electromagnetic Wave Scattering From Rough Terrain

1. INTRODUCTION

This determination of the electromagnetic scattering from rough terrain is divided into two aspects: the statistical analysis of the terrain features and the related electromagnetic calculation. The statistical part involves specification of terrain parameters by the use of estimation theory and characterization of the topographic heights by probability density functions (PDFs). The electromagnetic part applies some of the statistical results in a single-roughness-scale scattering calculation that will be compared to experimental data.

The characteristics of electromagnetic signals scattered from rough terrain include contributions from clutter return and multipath return.^{1, 2} These two aspects can be described by the theory of scattering from rough surfaces if properties of the terrain such as the PDF for the surface height distribution, the covariance matrix, R the variance in surface height, σ^2 and the complex dielectric constant characterizing the surface are known. The numerous theoretical models of EM wave scattering from rough surfaces¹⁻⁵ all relate the normalized cross section of terrain to the foregoing parameters characterizing the rough surface.

In our case, the physical parameters of the rough surface are obtained from digitized terrain maps (furnished by the Electromagnetic Compatibility Analysis

(Received for publication 29 October 1980)

(Due to the large number of references cited above, they will not be listed here. See References, page 32.)

Center, ECAC, and the Defense Mapping Agency, DMA). Estimation theory is employed to specify the corresponding statistical parameters. A hypothesis testing procedure determines the PDF for the surface heights.

The specific problem used as an example is that of characterizing a large terrain region considered to be made up of smaller subregions ($\sim 4 \text{ km}^2$). The main feature of interest is the distribution of heights within these subregions. Each subregion is characterized by a geologic code and several statistical parameters. In particular, we are concerned with being able to associate a PDF with the range of heights (z_i) in the subregions and to determine parameters that make the general PDF explicit. The data elements $z_i = z_i(x_k, y_l)$, where $i = 1, 2, 3, \dots, N$, and N is the total number of grid points in the x - y plane constituting the subregion. Here, x_k denotes the k^{th} equally spaced x -value along the x -axis and y denotes the l^{th} y -value along the y -axis, where $k = 1, 2, \dots, \sqrt{N}$ and $l = 1, 2, \dots, \sqrt{N}$. Thus, the N points are distributed in the x - y plane so as to form a rectangular grid. In this analysis, the covariance matrix can be assumed to have the form:

$$R_{mn} = \sigma^2 \exp(-\tau_{mn}^2 / T^2) \quad (1)$$

where

T = correlation length

and

$$\tau_{mn}^2 = (x_m - x_n)^2 + (y_m - y_n)^2$$

for the particular class of data sets used.

Motivation for assuming a covariance matrix of this form is that it leads to a tractable mathematical expression for the incoherent power that is scattered when an electromagnetic wave is reflected from a rough surface. Once the data have been used to specify the various parameters associated with possible distributions of heights in a region, several different methods have been developed to distinguish between distributions by means of a binary decision hypothesis testing procedure. In particular, the decisions involve whether certain Gaussian or exponential distributions are more appropriate for the observed heights. This specialization also is motivated by the theory of electromagnetic wave scattering from rough surfaces.^{1, 2}

The normalized radar cross section of the rough surface used in this study was derived by Hagfors,⁶ Barrick⁷ and Semenov.⁸ This cross section, σ_0 , is incorporated into a computer program that calculates the amount of specular and diffuse multipath power entering a monopulse receiver from a beacon located over rough terrain (see Figure 1). The computer program also calculates the error in boresight pointing accuracy of a monopulse receiving antenna due to noise and diffuse multipath. The computer program takes into consideration, among other things: (1) the spatial nonuniformity of the rough earth (that is, the preceding characterization parameters), (2) nonuniformities in the glistening surface, (3) finite pulse length of the beacon, (4) antenna elevation power pattern of the monopulse receiver, (5) multiple specular reflection points due to unevenness in surface heights, (6) interference between direct signal and multiple, specularly reflected signals, and (7) finite azimuthal beamwidth of transmitter and receiver. Finally, for the case of normally distributed surface heights, Sancer's⁹ results are employed to describe the effects of shadowing, and for the exponentially distributed case, Brown's¹⁰ backscatter shadowing calculation has been extended to handle the forward-scatter shadowing situation.

The results of the program describe the effect of the terrain on the electromagnetic signal. The final outputs include total coherent and diffuse power levels and the induced boresight error. The data output from the computer program for the sum pattern coherent power and angular error in boresight is compared with experimental data taken by personnel at the MIT Lincoln Laboratory Discrete Address Beacon System (DABS) test site.¹¹

6. Hagfors, T. (1964) Backscattering from an undulating surface with applications to radar returns from the Moon, J. Geophys. Res. 69:3779.
7. Barrick, D. E. (1968) Relationship between slope probability density function and the physical optics integral in rough surface scattering, Proc. IEEE 58:1728.
8. Semenov, B. I. (1965) Scattering of electromagnetic waves from restricted portions of rough surfaces with finite conductivity, Radiotekh, i Elektron 10:1952.
9. Sancer, M. I. (1969) Shadow-corrected electromagnetic scattering from a randomly rough surface, IEEE Trans. on Antennas and Prop. AP-17:577-585.
10. Brown, G. S. (1980) Shadowing by non-Gaussian random surfaces, Proceedings of the Second Workshop on Terrain and Sea Scatter, George Washington University, Washington, D. C.
11. McGarty, T. P. (1975) The Statistical Characteristics of Diffuse Multipath and its Effect on Antenna Performance, AD-A009889.

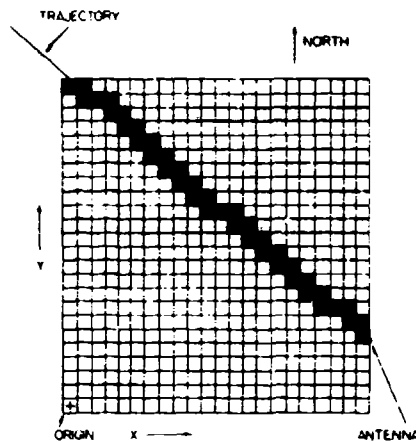


Figure 1. Boxes Along Trajectory Which Contribute to Specular and Diffuse Multipath

2. STATISTICAL ANALYSIS

For the statistical analysis of terrain heights in a region, our approach has been quite general. Depending on mission or system requirements, different approaches to such characterization may be more appropriate. Two specific formulations will be described; additional techniques are being investigated for future application. The two methods which we have formulated in detail are first, a single-observation multivariate-relation case and second, a bivariate time series approach. The results obtained by applying the first approach to a terrain data base will be presented here. The second is currently being applied to the same data base and those results eventually will be available for comparison.

2.1 Single Observation Formulation

The first approach involves a number of operations. At the outset, we propose some multivariate probability density functions that may represent the observed distribution of height values. Next, we use the available data to generate appropriate estimators of the parameters of the respective densities. Finally, we conduct a hypothesis test to ascertain which density function is more likely to have produced the observed height data.

The two PDF's for the heights are multivariate Gaussian or exponential. The Gaussian has a well-known form:¹²

12. Mood, A. M., and Graybill, F. A. (1963) Introduction to the Theory of Statistics, McGraw-Hill.

$$p(z'_1, z'_2, \dots, z'_N) = [(2\pi)^{N/2} |R|^{1/2}]^{-1} \exp\left(-\frac{1}{2} (\underline{z}' - \underline{\mu})^T R^{-1} (\underline{z}' - \underline{\mu})\right) \quad (2)$$

where R represents the covariance matrix. For our case, we assume equal means (μ) and equal variances (σ^2) and that the correlation function ($\rho_{ij} = \sigma_{ij}/\sigma^2$) has a Gaussian dependence on the separation between points. The next aspect is the development of a similar form for the exponential:

$$p_E(z'_1, z'_2, \dots, z'_N) = C_1 \exp(-C_2 [(\underline{z}' - \underline{\mu})^T R^{-1} (\underline{z}' - \underline{\mu})]^{1/2}). \quad (3)$$

The two coefficients (C_1, C_2) have to be determined. This will result in a form that satisfies the requirements for a PDF. To evaluate the coefficients, we use the properties that the zeroth moment integral of a PDF is equal to unity and that the second moment integral is equal to the variance. We thus obtain a form for the multivariate exponential:

$$p_E(z'_1, z'_2, \dots, z'_N) = [2^{\frac{N+1}{2}} (2\pi)^{\frac{N-1}{2}} \Gamma(\frac{N+1}{2}) |R|^{1/2-1}]^{-1} (N+1)^{\frac{N}{2}} \times \exp\left(-[(N+1) (\underline{z}' - \underline{\mu})^T R^{-1} (\underline{z}' - \underline{\mu})]^{1/2}\right). \quad (4)$$

In order to decide which of these two PDF's is more appropriate for the data, we must next establish estimators for parameters of the densities: the means, variance, and covariances. The complexity of correlated multivariate analysis and the computational limitations associated with the available data formats caused us to select estimators that have an intuitive appeal based on their form, rather than a rigorous derivation. From our assumption of equal means and variances, we use the sample mean as the estimator for the mean height and the sample variance as the variance estimate:

$$\hat{z} = (1/N) \sum_{i=1}^{\sqrt{N}} \sum_{j=1}^{\sqrt{N}} z(x_i, y_j) \quad (\text{mean}) \quad \text{and} \quad (5)$$

$$\hat{\sigma}^2 = (1/N) \sum_{i=1}^{\sqrt{N}} \sum_{j=1}^{\sqrt{N}} (z_{ij} - \hat{z})^2 \quad (\text{variance}). \quad (6)$$

The procedure for the covariance matrix estimators is more complicated. A correlation length, T, is defined as the separation at which a normalized covariance function C_{zz} had decreased to the value e^{-1} , where $C_{zz} = \gamma_{zz} \sigma^2$, and γ_{zz} is the estimator for the covariance. The data is used to determine the estimate of T in this fashion and then the complete covariance estimator is formed from the relation

$$\gamma_{zz}(m, n) = \sigma^2 \exp\left\{-\tau_{\text{inn}}^2 / T^2\right\} \quad (7)$$

(separate x and y relations are calculated). The form of the covariance (x direction) used to determine T is

$$\hat{C}_{zz}(k) = (1/N\sigma^2) \left[\sum_{j=1}^{\sqrt{N}} \sum_{i=1}^{\sqrt{N}-k} z_{ij} z_{i+k,j} - \frac{\hat{\mu}^2}{2} \sum_{j=1}^{\sqrt{N}} \sum_{i=1}^{\sqrt{N}-k} z_{ij} - \frac{k^2 \hat{\mu}^2}{\sqrt{N}} \right] \quad (8)$$

where k represents the separation distance. A least-squares-fit of the C_{zz} values to a parabola is then used to find T. Under the assumptions that have been made, the above estimators are similar to those found in Jenkins and Watts.¹³ Values for T in the x and y directions were obtained, and then the two values averaged to find the final estimate of T in a given subregion.

We now have the two PDF forms and the required parameters. The next aspect is to decide which PDF is the more appropriate for the given data. One final comment on the parameters: In order to satisfy the restrictions of the PDF's, it is necessary to show that the quadratic form appearing in both cases is positive definite. This has been demonstrated for the foregoing cases by making use of the Gaussian form assigned to the covariance matrix elements. Details can be found in the report by Lennon and Papa.¹⁴

The form of the hypothesis test used here is based on the maximum a posteriori probability criterion. This is equivalent to a minimum error probability criterion. We assign hypothesis H_1 to the Gaussian case and hypothesis H_0 to the exponential. Then the likelihood ratio parameter,

$$\lambda \triangleq p_1(z_1, z_2, \dots, z_N) / p_0(z_1, z_2, \dots, z_N). \quad (9)$$

Let $P(H_0)$ be the probability that hypothesis H_0 is true. Then the decision rule may be written as: Choose H_1 if

$$\lambda \geq \frac{P(H_0)}{1 - P(H_0)}. \quad (10)$$

For our case, we assume that it is equally probable that hypothesis H_1 or H_0 is true and the decision rule reduces to whether or not $\lambda \geq 1$. Note that it may be

13. Jenkins, G. M., and Watts, D. G. (1968) Spectral Analysis and its Applications, Holden-Day.

14. Lennon, J. F., and Papa, R. J. (1980) Statistical Characterization of Rough Terrain, RADC-TR-80-9, RADC/EE Hanscom AFB, Massachusetts.

possible to alter the probability that H_0 is true based on external evidence (such as the type of terrain).

When the specific forms for the two PDF's are introduced into this relation it becomes

$$\lambda = (P_1/P_0) = \left(\frac{\Gamma\left(\frac{N+1}{2}\right) \exp\left(\frac{N+1}{2}\right)}{\sqrt{\pi} \left(\frac{N+1}{2}\right)^{N/2}} \right) \exp\left(-\frac{1}{2}(Q - \sqrt{N+1})^2\right) \quad (11)$$

where

$$Q = [(z - \mu)^T R^{-1} (z - \mu)]^{1/2}.$$

For convenience, we rewrite the test in logarithmic form and obtain the result that H_1 is true if either

$$Q \leq \left\{ \left[2 \ln \left(\Gamma \left(\frac{N+1}{2} \right) \right) + (N+1) - \ln \pi - N \ln \left(\frac{N+1}{2} \right) \right]^{1/2} + \sqrt{N+1} \right\} \quad (12)$$

or

$$Q \geq \left\{ \sqrt{N+1} - \left[2 \ln \left(\Gamma \left(\frac{N+1}{2} \right) \right) + (N+1) - \ln \pi - N \ln \left(\frac{N+1}{2} \right) \right]^{1/2} \right\}. \quad (13)$$

For the actual cases, $N = 100$, and the specific result is our decision that the terrain heights in a given region are from a Gaussian PDF if

$$85.01 \leq [(z - \mu)^T R^{-1} (z - \mu)] \leq 118.37$$

and conversely the points are exponential if $Q^2 > 118.37$ or $Q^2 < 85.01$.

2.2 Multiple Observation Formulation

The second approach to statistical characterization of terrain heights eliminates the need for matrix inversion by dealing with the points as successive sets of pairs. This allows us to use a bivariate form of the probability density function (PDF) when constructing the hypothesis test. This new approach is aimed at characterizing the relations between pairs of points in a region where we assume isotropy and stationarity in the height distribution. This is an appropriate characterization, since the related electromagnetic calculation is concerned with the mean value of the scattered power.

The two-point characterization is a supplement to the original N-variate result; it is from the standpoint of calculation more appealing and should give better results

by avoiding the problems of inverting large matrices and by introducing a form that allows multiple observations, rather than a single multivariate observation.

As in the foregoing discussion two basic types of analysis are involved: (1) the determination of appropriate estimators; and (2) a hypothesis test using PDF's based on the estimators. This introduces one complication; that is, the estimators are always based on summations involving $N = 10$, whereas the test uses subsets of points in sums with two limits, $K = 48$ and $S = 16$; K is the number of different pair spacings to be considered and S the number of observations at each spacing.

The estimators for the means and variances are the same as those described in the first approach. For the covariance estimation, however, the situation is different. We now form a distinct estimator for each separation: $C(r)$, where r is an index assigned to the combined (a, b) grid spacing.

Numerical values for indices in the following sections correspond to the specific case where the method has been applied to the ECAC data base. The values of r are $r = 0, 1, 2, \dots, K = 48$; $C(r)$ is assigned to $C(a, b)$ according to the scheme described below, but this is arbitrary and other orderings could be used. There are thus 49 covariance estimators since the x and y coordinate spacings on the grid differ and we allow $a = 0, 1, 2, 3, 4, 5, 6$ and $b = 0, 1, 2, 3, 4, 5, 6$ where $a \Delta x$ is the x coordinate separation and $b \Delta y$ is the y coordinate separation for the two points of the pair. The number of possible pairs at a given separation (a, b) is $(N-a) \times (N-b)$. Thus for $a = 0, b = 0$, there are 100 possible pairs, $(z_{pq}, z_{p+a, q+b})$ and for $a = 6, b = 6$, there are 16 possibilities. Then by assigning each of the 49 r -values to a particular (a, b) combination we have:

$$C(r) = C(a, b) = \left[\left(\frac{1}{N^2 \sigma^2} \right) \left(\sum_{p=1}^{N-a} \sum_{q=1}^{N-b} z_{pq} z_{p+a, q+b} \right) + \left(\frac{(N-a)(N-b) \bar{z}^2}{N^2 \sigma^2} \right) - \frac{\bar{z}}{N^2 \sigma^2} \left(\sum_{p=1}^{N-a} \sum_{q=1}^{N-b} (z_{pq} + z_{p+a, q+b}) \right) \right] \quad (14)$$

where for convenience we assign:

$C(0) \rightarrow C(0, 0);$	$C(1) \rightarrow C(0, 1);$...	$C(6) \rightarrow C(0, 6);$
$C(7) \rightarrow C(1, 0);$	$C(8) \rightarrow C(1, 1);$...	$C(13) \rightarrow C(1, 6);$
..... ;	$C(27) \rightarrow C(3, 6);$;	
$C(41) \rightarrow C(5, 6);$;	and	$C(48) \rightarrow C(6, 6).$

(Note that with this notation $C(0) = C(0, 0) = 1$. This is consistent.)

At this point we have all the necessary estimators for use in the hypothesis test and we could proceed directly to that aspect. However, for the electromagnetics, it is still desirable to determine the correlation length T , in a similar fashion to the original case, although it will not be used in the statistics. We already have our $C(r)$ values defined, so we set $d^2(r) = (a \Delta x)^2 + (b \Delta y)^2$ and obtain as before:

$$T = \left[\left(1 - e^{-1} \right) \left(\frac{\sum_{r=1}^{48} d^4(r)}{\sum_{r=1}^{48} d^2(r) - \sum_{r=1}^{48} d^2(r) C(r)} \right) \right]^{1/2} \quad \text{in meters.} \quad (15)$$

The next topic is that of the hypothesis test. Here, as we pointed out before, each r value will use only $S = 16$ cases. For $(a = 6, b = 6)$ there are only 16 possible pairs of $(z_{pq}, z_{p+a, q+b})$, but for all the other cases there are additional possibilities. Some scheme has to be used [that is, random number generation, or selection from a broad range of (p, q) values] so that a representative selection of pairs are used in the test for each r value.

The hypothesis test is similar to the previous form but in this case we have multiple observations and so the probabilities with which we are concerned are the likelihood functions for the respective bivariate probability densities. Since we are dealing with multiple observations, it should be noted that in the following relations, the superscripts identify the two $z_{p, q}$ or $z_{p+a, q+b}$ members of the pair, whereas the subscripts r and i now refer to the separation and selection number, respectively.

For the Gaussian case

$$P_1 = \left(\frac{1}{2\pi\sigma^2} \right)^{KS} \left[(1 - C^2(1))(1 - C^2(2)) \cdots (1 - C^2(K)) \right]^{-\frac{S}{2}} \\ \times \exp \left\{ - \left[\left(\frac{1}{2\sigma^2} \right) \sum_{r=1}^K \sum_{i=1}^S \left(\frac{(z_{ri}^{(1)} - \bar{z})^2 - 2C(r)(z_{ri}^{(1)} - \bar{z})(z_{ri}^{(2)} - \bar{z}) + (z_{ri}^{(2)} - \bar{z})^2}{1 - C^2(r)} \right) \right] \right\} \quad (16)$$

For the exponential case

$$P_0 = \left(\frac{3}{2n\sigma^2} \right)^{KS} \left[(1 - C^2(r))(1 - C^2(2)) \cdots (1 - C^2(K)) \right]^{-\frac{S}{2}} \\ \times \exp \left\{ - \left[\sqrt{\frac{3}{\sigma^2}} \sum_{r=1}^K \sum_{i=1}^S \left(\frac{(z_{ri}^{(1)} - \bar{z})^2 - 2C(r)(z_{ri}^{(1)} - \bar{z})(z_{ri}^{(2)} - \bar{z}) + (z_{ri}^{(2)} - \bar{z})^2}{1 - C^2(r)} \right)^{\frac{1}{2}} \right] \right\} \quad (17)$$

These terms are then introduced into the hypothesis test and simplified by formation of the log-likelihood function, which leads to the following decision: Choose a Gaussian PDF when $TEST \leq SK (3-2 \ln 3) \sigma^2$. This becomes

$$\left[\sum_{r=1}^{48} G(r) \right] - 617\sigma^2 \leq 0$$

where

$$G(r) = \sum_{i=1}^{16} \left[\left(\frac{(z_{ri}^{(1)} - \bar{z})^2 - 2C(r)(z_{ri}^{(1)} - \bar{z})(z_{ri}^{(2)} - \bar{z}) + (z_{ri}^{(2)} - \bar{z})^2}{1 - C^2(r)} \right)^{1/2} - \sqrt{3\sigma^2} \right]^2. \quad (18)$$

The results for this approach are not yet available. The single observation, multivariate characterization is thus the only one that can be used as an input to the electromagnetic calculations.

3. SITE CHARACTERIZATION

The specific site used for the characterization is one in eastern Massachusetts.¹¹ This area was selected because of the availability of electromagnetic terrain scattering data obtained during tests of a beacon system at that location. A rectangular area around this Discrete Address Beacon System (DABS) site was designated. The rectangular area was 43.3 km long and 42.8 km wide. The area was then subdivided into smaller rectangular cells, each with sides of 2050 m by 1825 m. Each cell is further subdivided into a 10 by 10 grid of points. A data base of topographic elevations for this area is available at the Electromagnetic Compatibility Analysis Center (ECAC). This was prepared from Defense Mapping Agency (DMA) supplied digitized terrain maps at 1: 250,000 scale size.

The statistical data for each cell has been recorded on a computer tape for use with the program for the electromagnetic analysis. Each cell is represented by seven descriptors. The first two entries are the (x, y) coordinates for the center of the cell. (The origin of the coordinate system is taken as the center of the extreme southwestern corner of the rectangular region.) The next item is the geological code for the cell. The predominant feature is woods; there are a number of cells containing clusters of lakes and ponds and a few town sites with associated cleared areas. This is followed by the mean and variance of the heights in the cell and the estimated correlation length, τ (the units of length are in meters). The final quantity is the result of the hypothesis test. This result is presented in a

format such that the heights in a region are Gaussian when $(-33.36 \leq \text{TEST} \leq 0)$. When $\text{TEST} = 0$ and the variance is very small, the region is essentially a smooth surface (no roughness).

When the over-all results for the region are examined,¹⁴ one observation that can be made is that when the magnitude of TEST is very large, the correlation length is also very large; for those cases T is comparable to one half the cell size or even larger. When that occurs, the determinant of the covariance matrix, R , becomes very small. As a result, it is increasingly difficult to obtain an accurate inverse of R , due to rapid build-up of round-off error. It should be noted here that the second characterization technique is based on bivariate formulation, so the inverse of R is introduced analytically. Hence, in that case, the round-off errors of the machine-calculated inverse do not enter the result. A related difficulty in the results of the first approach can be seen in those cases where $\text{TEST} < -118.37$. This would be possible only if the quadratic form Q^2 is not positive definite. This contradiction of that theoretically imposed requirement implies that further machine-induced errors were present and those results can not be considered valid.

The grid structure for the site in Massachusetts has been analyzed in terms of specific trajectory of the test program in an attempt to obtain a quick correction of the hypothesis test results. The actual subset of boxes that contribute to the specular and diffuse scattering analysis for the trajectory are shown in Figure 1. For those cases, the analysis was reproduced on a more accurate computer and a second set of TEST results were obtained. This second set did not suffer from the extreme round-off problems of the original calculation. These results have been used in the present comparisons.

In order to use these results in the rough surface electromagnetic calculations, one additional aspect should be noted. For the types of geological features that describe the respective regions, data exist on the associated complex dielectric constants at microwave frequencies.^{15, 3}

4. ELECTROMAGNETIC SCATTERING ANALYSIS

The radar cross section of terrain is normalized with respect to the average area illuminated by the radar. The normalized cross section, σ_0 , may be divided

14. Lennon, J. F., and Papa, R. J. (1980) Statistical Characterization of Rough Terrain, RADC-TR-80-9, RADC/EE Hanscom AFB, Massachusetts.
15. Lytle, R. J. (1974) Measurement of earth medium electrical characteristics: Techniques, Results and Applications, IEEE Trans. on Geoscience Electronics, GE-12:81

into three general categories: (1) the slightly rough surface;¹⁶ (2) the very rough surface,^{1, 6, 7, 8} and (3) the multiple scale rough surface.^{17, 18, 4} This study deals with the second category, that is, the very rough surface (irregularities are large compared to a wavelength). Fine scale effects are introduced cursorily by the use of effective complex dielectric constants assigned on the basis of geologic descriptors in each terrain region (lakes, woods, roads, and so on). This is an adequate model for the forward scattering problem associated with beacon transmission, but for cases where backscatter results are of interest the fine scale contributions have to be considered in greater detail.

This is justified for the following reason. At low incident grazing angles, the large, gently undulating irregularities will tend to scatter in the forward direction and represent the dominant contribution in that direction. The fine scale roughness (where irregularities are small compared to a wavelength) will tend to scatter energy in directions satisfying the Bragg conditions, as modified by the large scale tilting effects. These fine scale results will dominate in the backscatter region, where there are only secondary large scale roughness contributions, but only represent a secondary contribution to the complete forward scatter result.

4.1 Scattering Cross Section

Ruck et al² give expressions for the average bistatic rough surface cross section σ_0 under the following four assumptions: (1) the radius of curvature of the surface irregularities is larger than a wavelength; (2) the roughness is isotropic in both surface dimensions; (3) the correlation length is smaller than either the x or y dimension of the sample subregion; and (4) multiple scattering is neglected. Using the notation of Ruck et al,² one finds that the expression for σ_0 becomes

$$\sigma_0 = |\beta_{pq}|^2 J \quad (19)$$

where

$$J = (T^2/\sigma^2 \xi_z^2) \exp \left[- \left(\frac{T^2}{4 \sigma^2} \right) \left(\frac{\xi_x^2 + \xi_y^2}{\xi_z^2} \right) \right]$$

16. Peake, W. H. (1959) The Interaction of Electromagnetic Waves With Some Natural Surfaces, Antenna Laboratory, Ohio State University, Report No. 898-2.
17. Wright, J. W. (1968) A new model for sea clutter, IEEE Trans. on Antennas and Prop. AP-16:217-223.
18. Fuks, I. (1966) Contribution to the theory of radio wave scattering on the perturbed sea surface, Iz. Vyssh. Ucheb. Zaved. Radiofiz., 5:876.

for a Gaussian bivariate surface height probability density function and

$$J = (3T^2/\sigma^2 \xi_x^2 \xi_z^2) \exp \left[- \left(\frac{\sqrt{6} T}{2\sigma} \right) \left(\frac{\xi_x^2 + \xi_z^2}{\xi_y^2} \right)^{1/2} \right] \quad (20)$$

for an exponential surface height probability density function. The scattering matrix elements β_{pq} are given by

$$\begin{aligned} \beta_{vv} &= \frac{(1 + \cos 2\alpha) R_{\parallel}(\alpha)}{(\cos \theta_i + \cos \theta_s)} && \text{(vertical polarization)} \\ \beta_{hh} &= \frac{(1 + \cos 2\alpha) R_{\perp}(\alpha)}{(\cos \theta_i + \cos \theta_s)} && \text{(horizontal polarization)} \\ R_{\parallel}(\alpha) &= \frac{\epsilon_r \cos \alpha - \sqrt{\epsilon_r - \sin^2 \alpha}}{\epsilon_r \cos \alpha + \sqrt{\epsilon_r - \sin^2 \alpha}} \\ R_{\perp}(\alpha) &= \frac{\cos \alpha - \sqrt{\epsilon_r - \sin^2 \alpha}}{\cos \alpha + \sqrt{\epsilon_r - \sin^2 \alpha}} \\ \xi_x &= \sin \theta_i - \sin \theta_s & \xi_y &= 0 & \xi_z &= -\cos \theta_i - 1.0 \end{aligned}$$

where

θ_i = angle of incidence (with respect to surface normal)

θ_s = angle of scattering (with respect to surface normal)

and

$$\alpha = \left(\frac{\theta_i + \theta_s}{2} \right).$$

Here, ϵ_r is the relative complex dielectric constant of the surface, the subscript \parallel refers to the E-field in the plane of incidence, and the subscript \perp refers to the E-field normal to the plane of incidence. These simplified forms of Ruck's expressions follow from the assumption that the receiver is far from the transmitter so that the portion of the "glistening surface"¹ that contributes to the diffuse multipath is a long, narrow strip extending between transmitter and receiver. This assumption allows us to make the approximation that the azimuthal scattering angle, $\phi_S \approx 0.0$. This will be further discussed in Section 4.5.

4.2 Shadowing

The effect of shadowing on the diffuse scatter from the surface is introduced by multiplying the expression for σ_0 by an appropriate shadowing function, depending on whether the surface heights of the particular contributing subregion are normally or exponentially distributed.

In this study, Sancer's⁹ results are used to describe the effects of shadowing when the surface heights are normally distributed. For the situation where the surface heights are exponentially distributed, Brown's¹⁰ expressions for shadowing in the case of backscattering have been extended to include shadowing in the forward scattering direction. The details of the exponential shadowing formulation are presented in Appendix A.

4.3 Program Initiation

The computer program is designed to incorporate the expression for σ_0 into an integral over the glistening surface. The program has the capability of calculating the coherent power (specular plus direct) and diffuse multipath power reaching a monopulse receiver from a beacon over rough terrain (Figure 2). The computer program uses the previously described data tape of the statistical parameters for a particular site as an input. Other input variables characterize the transmitter, the environmental aspects, and the receiver. Transmitter values include: the gain of the transmitter, the polarization of the transmitted wave, the peak power of the transmitted pulse, the pulse length, and the wavelength of the signal. External inputs include: the complex dielectric constant of each type of geological region, the coordinates (latitude and longitude) of the monopulse receiver, the initial and final position of the aircraft containing the transmitter, a parameter to control the effects of shadowing, and the velocity of the aircraft. Receiver data include: the height of the receiver, the bandwidth of the receiver, the front-end receiver-noise figure, the antenna gain for the sum and difference patterns of the monopulse receiver, its azimuthal beamwidth, the sampling frequency of the receiver, the transmission line loss factor of the cables connecting the antenna to receiver, and the difference pattern slope near the boresight axis.

From a knowledge of the initial and final positions of the aircraft and the aircraft speed, the computer program first calculates the trajectory, as a function of time. Then, from a modified form of the radar range equation, the electric field intensity of the direct signal at the receiver is calculated at fixed time intervals (sampling time is an input variable to the program).

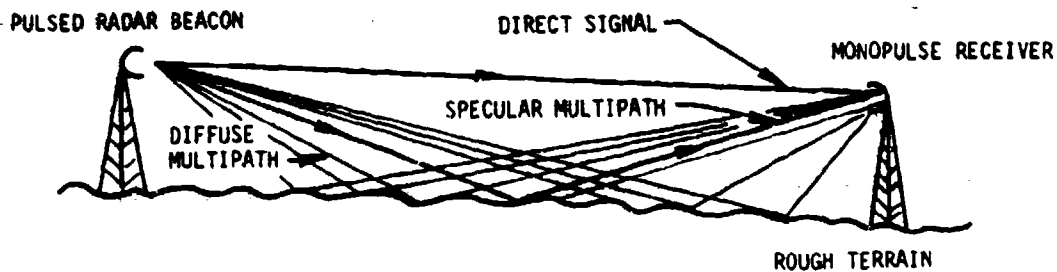


Figure 2. Reflection of Radar Waves From Rough Terrain

4.4 Specular Multipath

For the specular multipath rays, all possible specular reflection points between the transmitter and receiver are determined from each position of the transmitter. Multiple specular reflection points due to unevenness in surface height are taken into consideration. At each possible point, the path to both antenna and transmitter is examined for ray blocking by the surface heights along the trajectory. The appropriate finite dielectric constant of the earth at each specular point, the antenna elevation pattern (receive) and the surface roughness are also accounted for in calculating the phase and amplitude of each specular multipath ray. At each point on the transmitter's trajectory, the total coherent power for the sum and difference channels in the monopulse receiver is calculated.

One aspect of the discussion of specular multipath that relates to the magnitude of the effect as a function of range is the extent of the contributing region. Figure 3 shows the history of the region as the target approaches the receiving antenna. For this analysis, the first Fresnel zone is considered the area from which specular reflections can occur and the remaining zones are assumed to cancel each other. The curves depict the specular point location, the center of the Fresnel zone, and its extent and width. Details of these calculations are included in Appendix B and the significance of the results is analyzed in Section 5.

4.5 The Glistening Surface

In the calculation of the total diffuse power, account is taken of spatial inhomogeneities of the rough earth and nonuniformities in the boundaries of the glistening surface. In Figure 4, a typical illustration is given of this surface. The distance from the receiver to the edge of the glistening surface is l_1 , and the distance from the transmitter to the opposite edge of the surface is denoted l_2 . These distances are a function of the ratio σ/T , and explicit expressions for them are given by Benckmann and Spizzichino.¹ For the system and environmental parameters being

investigated in this report, it was found from computational experiments that significant additional contributions to the diffuse power originated from regions beyond the classical definition of the glistening surface. To allow for this, the expressions for l_1 and l_2 were modified so as to extend the length of this glistening surface. In calculating the total diffuse power, the normalized cross section σ_o is integrated over the glistening surface. Since the terrain is inhomogeneous, the integration is accomplished by dividing the surface into small strips, as shown in Figure 4. The total diffuse power is calculated by summing the contributions from each strip.

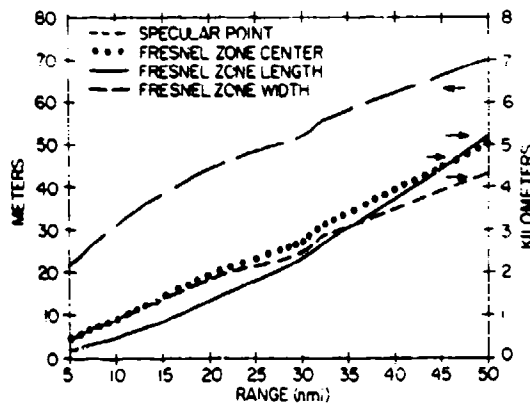


Figure 3. Fresnel Zone Dimensions

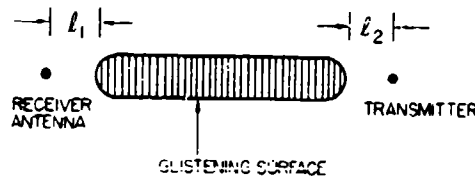


Figure 4. The Glistening Surface

4.6 Diffuse Multipath

The diffuse multipath power, P_{DIFF} , entering the receiver is obtained from the equation:

$$P_{DIFF} = \frac{P_T \lambda^2 G_{TR}^{AZ}}{(4\pi)^3} \iint \left(\frac{G_{TR}^{EL}(\theta_1) G_R^{EL}(\theta_2) G_R^{AZ}(\theta_2) \sigma_o}{R_1^2 R_2^2} \right) dS$$

where

- P_T = transmitted power,
 λ = wavelength,
 G_{TR}^{AZ} = gain (power) of transmitter in azimuth,
 G_R^{AZ} = gain of receiver in azimuth,
 G_{TR}^{EL} = gain of transmitter in elevation,
 G_R^{EL} = gain of receiver in elevation,
 θ_1 = angle between boresight and point on glistening surface for transmitter,
 θ_2 = angle between boresight and point on glistening surface for receiver,
 R_1 = range between transmitter and point on glistening surface,
 R_2 = range between receiver and point on glistening surface,
 dS = element of area of glistening surface which is illuminated by beacon

In the numerical integration of the equation for P_{DIFF} , the transmitter is assumed to have a uniform azimuthal power pattern and the azimuthal variation in σ_0 has been assumed negligible. Two different cases were considered for the azimuthal power pattern variation of the receiving antenna. First, it was assumed to be constant at 5 dB below the sum pattern gain. This gain corresponds to 3 dB below the peak in the difference gain. In a more refined analysis, the power pattern was described by a parabolic dependence on azimuthal angle and treated as a variable in the integration over the power pattern. The details of this azimuthal power pattern variation are presented in Appendix C.

4.7 Boresight Error

To calculate the error in boresight of the monopulse receiver due to diffuse multipath and receiver noise, it is assumed that the diffuse multipath is decorrelated from pulse to pulse and that the spectral width of the diffuse multipath power is narrow compared to the bandwidth of the receiver/processor. These assumptions appear to be justified on the basis of rough, order-of-magnitude estimates of the appropriate parameters. Under these assumptions, the total amount of noiselike interference is given by

$N_I = P_{DIFF} + N_o$, where

N_I = noiselike interference power

N_o = noise power from environment plus receiver.

The error, σ_θ , in azimuthal boresight pointing accuracy is given by the expression from Barton and Ward¹⁹ as follows:

$$\sigma_\theta = \frac{\theta_B}{k_m \sqrt{2 \text{ STIR}}}$$

where

θ_B = azimuthal beamwidth,

STIR = P_{coh}/N_I = signal to interference ratio in the difference channel,

P_{coh} = coherent power,

k_m = normalized monopulse slope (obtainable from sum and difference patterns).

The output of the computer program consists of azimuthal angular error in boresight due to noise, the error due to noise plus diffuse multipath, the total sum pattern coherent power, the total diffuse power, signal-to-noise ratio, signal-to-interference ratio, and range from transmitter to receiver. In the conclusions, the computer output for the analysis of a particular site is compared with some experimental data.

5. RESULTS AND CONCLUSIONS

Two theoretical results, the coherent power in the sum channel of a monopulse antenna, P_{coh} , and the standard deviation in boresight pointing accuracy, σ_θ , are compared with the experimental data of McGarty,¹¹ taken at the DABS site.

5.1 Experimental Conditions

The DABS receiver was an L-band rotatable array. The beacon was located on a U-10 aircraft which flew a number of radial trajectories toward and away from the monopulse receiver. Data were recorded for about 100 flights for different

19. Barton, D. K., and Ward, H. R. (1969) Handbook of Radar Measurement, Prentice-Hall.

aircraft heights, different radial flight trajectories, and different receiver-antenna tilt angles. The conditions under which the data were taken are listed in Table 1.

Table 1. Experimental Conditions for DABS Tests

Front end receiver noise figure	3 dB
Gain of monopulse receiver (sum pattern)	22.5 dB
Gain of transmitter	4 dB
Height of receiver	101 m
Height of transmitter	1220 m
Signal polarization	vertical
Peak transmitter power	350 W
Pulse length	20 μ sec
Azimuthal beamwidth (receiver)	3°
Wavelength	0.275 m
Transmission line loss factor	3 dB

In order to make the comparisons, various manipulations were required. In the equation for σ_θ , the normalized slope in the difference pattern near boresight, k_m , was obtained from graphs of the sum and difference patterns of the monopulse antenna. Within the accuracy of these graphs, it appears that ($1.5 \leq k_m \leq 1.7$). Figures 5 and 6 present experimental data with which various theoretical results are to be compared. Figure 5 is a plot of the sum signal (P_{coh}) versus range of transmitter to receiver in nmi. Figure 6 is a plot of azimuth error (σ_θ) versus range in nmi.

5.2 Coherent Power Results

The magnitude of the coherent power multipath contribution from specularly reflected rays depends on the relationship of the specular region to the variance and correlation length, as well as the over-all size of the specular region used in the calculation. The effect of these aspects on the nature of the coherent results is significant.

It should be recalled that Figure 3 shows the extent of the first Fresnel zone decreasing as the range from transmitter to receiver decreases. Figure 1 illustrates all the boxes along the trajectory that contribute to the specular and diffuse multipath power; the actual boxes that contribute to the result in a given case depend on the position of the transmitter along the trajectory. In particular, for the range of system and environmental parameters under investigation in this report,

only the three boxes closest to the receiving antenna (in the southeastern corner of the total region.) contribute to the specular reflections. Also, for each position of the transmitter, there is only one specular reflection point.

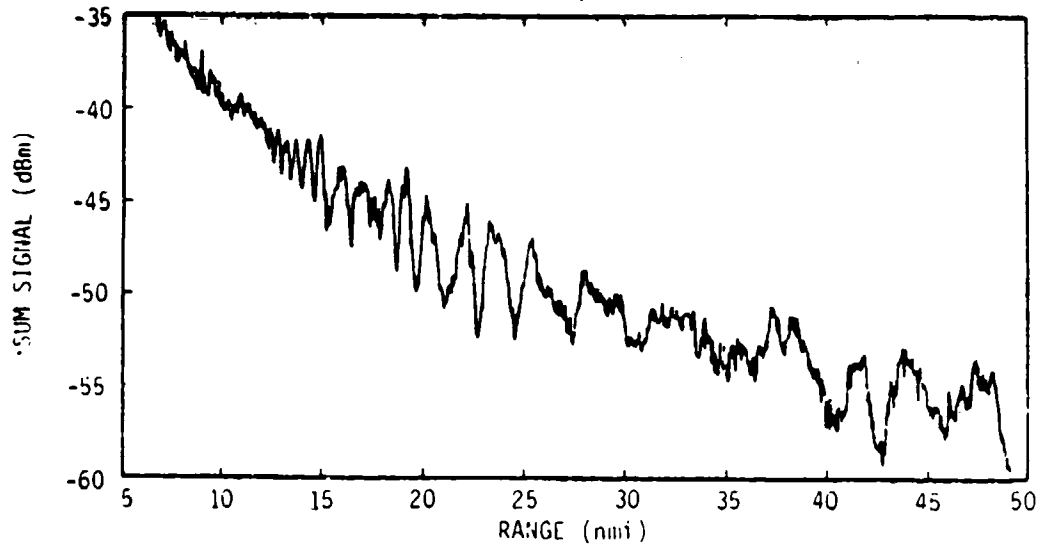


Figure 5. Experimental Data: Sum Signal (P_{coh}) vs Range

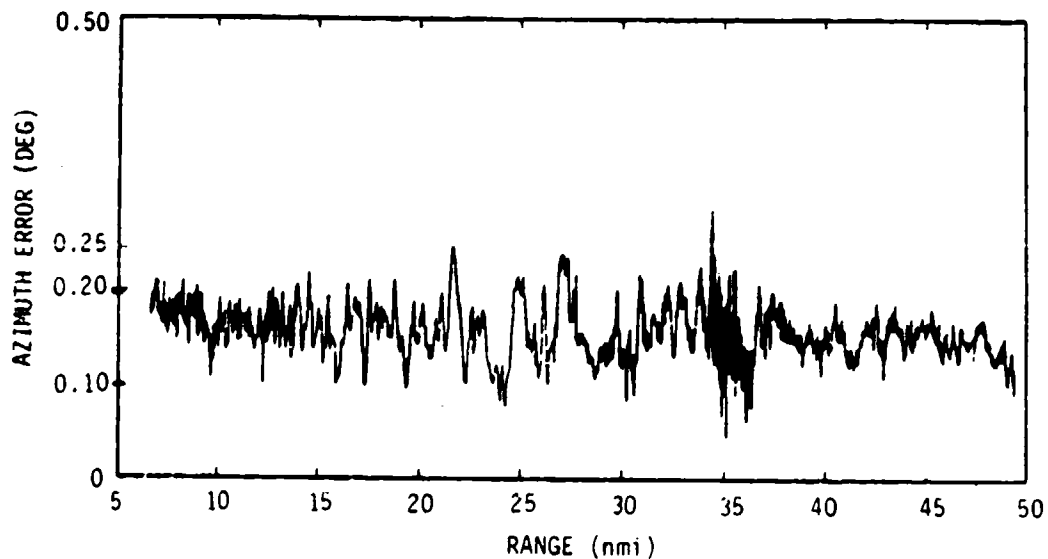


Figure 6. Experimental Data: Azimuthal Error (σ_θ) vs Range

Initially, the variance associated with the distribution of heights over an entire box (see Figure 1) was used in the Rayleigh attenuation factor of the specular multipath ray. The coherent power from the specularly reflected rays is small in that case and the result is just the direct-ray ($1/R^2$) fall off of power with range R. This result is not inconsistent with what would be expected when the size of the actual contributing region (on the order of the first Fresnel zone) is considered, along with the associated assumption of small correlation length contained in the scattering formulation. When the first Fresnel zone's dimensions are considerably smaller than the box size (2 km by 2 km), smaller sample regions should be used in calculating the variances in surface height.

The calculation of more localized variances associated with the Fresnel zone dimensions was then performed. This resulted in smaller values for the variances and increased specularly reflected multipath power. Figure 7 shows the calculated coherent power for the sum signal, together with the actual data. The specular contributions were calculated using variances based on trajectory-centered sub-regions of the three boxes closest to the antenna. As the specular point shifts across the three regions, the effect of the different values for the three local variances can be seen in successive changes that appear in the behavior of the signal. The theoretical results tend to be about 6 dB higher on the average; this is most likely due to the fact that the receiver/processor losses are unknown and hence have been neglected. When typical processing losses of -5 dB are included in the analysis, the calculated coherent power for the sum signal, together with the actual data, are in remarkable agreement, as may be seen from Figure 8.

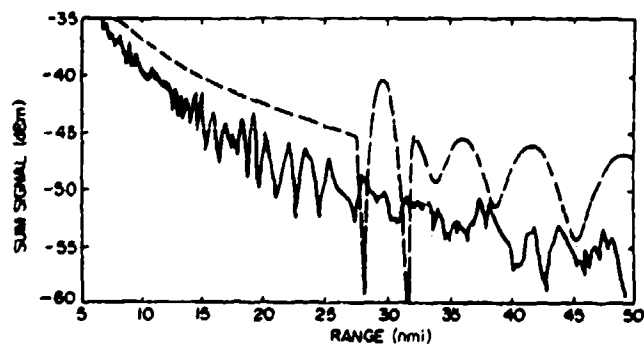


Figure 7. Theoretical Calculations and Experimental Data: Sum Signal vs Range

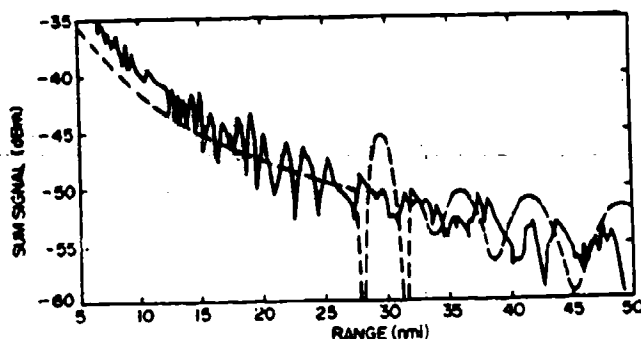


Figure 8. Theoretical Calculations and Experimental Data: Sum Signal vs Range (system losses = -5 dB)

It should be noted that the usual expression for the Rayleigh attenuation factor of the specularly reflected ray (as given by Beckmann and Spizzichino)¹ was derived by assuming that the correlation length T is much smaller than the dimensions of the Fresnel zone. For close ranges, the parameters investigated in this report are such that T becomes comparable to the dimensions of the Fresnel zone. In this case, additional corrections have to be made for the specularly reflected ray. This problem area is currently being investigated.

5.3 Boresight Error Results

Before specific results are addressed, some general comments should be made. First, for the range of parameters used in this analysis, the inclusion of shadowing in the boresight error calculation does not introduce a significant change from the cases where shadowing is neglected. Second, unlike the coherent power results, present results extend to a maximum of only 30 nmi (the trajectory originates at 50 nmi). The coherent results are affected only by the area close to the receiving antenna whereas the glistening surface extends over a considerable extent of the trajectory for the diffuse multipath power. Therefore, the finite nature of the geographical data base limited the farthest point at which the diffuse contributions could be assessed. Finally, it should be noted that these results do not include any fine scale roughness contributions to the diffuse power.

The figures show the variation in calculated boresight error as a function of range. These results reflect a wide range of parameters and assumptions about different aspects of the analysis. First, we vary k_m and the PDF of the surface heights. For both these cases, the results shown are for a model that assumes

there is an average 18.5 dB gain over the 3° beamwidth of the monopulse difference pattern.

In Figure 9, σ_θ is plotted versus range for exponentially distributed surface heights where $k_m = 1.5$, processing losses of -5 dB are included, and the effects of shadowing are taken into account. Comparison of Figure 9 with Figure 6 shows that the theoretical boresight errors, σ_θ are somewhat less than the experimental values.

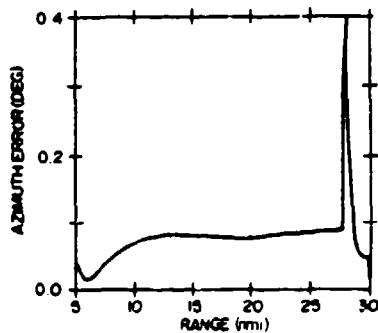


Figure 9. Theoretical Calculations: σ_θ vs Range, $k_m = 1.5$, Shadowing, Exponential PDF

Figure 10 has the same parameter values as Figure 9, except that $k_m = 1.7$, instead of $k_m = 1.5$. Comparison of Figure 10 with Figures 9 and 6 shows that the higher value for k_m results in slightly poorer agreement between theory and experiment. In conclusion, there is no significant effect on σ_θ for the range of k_m values used here.

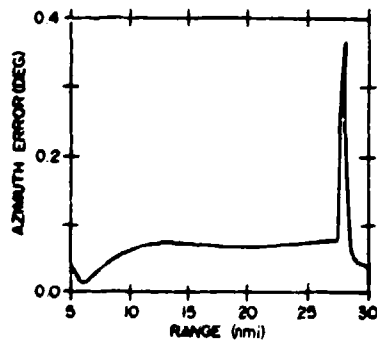


Figure 10. Theoretical Calculations: σ_θ vs Range, $k_m = 1.7$, Shadowing, Exponential PDF

All the parameters in Figure 11 are identical with those in Figure 9, except that the PDF for the surface heights is Gaussian, instead of exponential. Comparison of Figure 11 with Figure 9 shows: The assumption that the surface heights are all normally distributed results in less diffuse multipath power entering the receiver, with a consequent decrease in the boresight error.

These two conditions represent the extremes of the possible effects of surface height distribution on boresight error for these two PDF's. The initial statistical analysis of the terrain heights in the boxes along this particular trajectory leads to the conclusion that the exponential PDF was most appropriate in all instances. Thus, that statistical model asserts that the results of Figure 9 and Figure 10 are the ones to consider rather than those of Figure 11. Additional statistical approaches (including the multiple observation bivariate formulation) are being examined to assess their conclusions for the PDF's of these same regions.

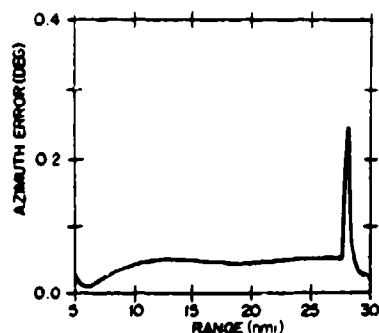


Figure 11. Theoretical Calculations: σ_θ vs Range, $k_m = 1.5$, Shadowing, Normal PDF

The next effect to be examined is the inclusion of an azimuthal variation in the difference channel power pattern instead of an average value. This is discussed in Appendix C. Figure 12 shows this result. Here, $k_m = 1.5$, the surface height PDF is assumed to be exponential, and the effects of shadowing are included. Comparison of Figure 9 with Figure 12 shows that the inclusion of the azimuthal variation in power pattern results in a decrease in diffuse multipath power and a decrease in boresight error σ_θ . This is due to the fact that the width of the glistening surface as defined in Beckmann and Spizzichino¹ is very narrow (approximately 40 m or about 0.1° angular extent). The calculation thus uses an average difference pattern gain over this angular region ≈ 20 dB below the sum channel gain. On the other hand, in the approximation that there is no azimuthal variation in power pattern, the value of 5 dB below the sum channel gain is used as the average. This accounts for the decrease in diffuse power and boresight error when the actual azimuthal variation is included.

Finally, by comparing Figure 6 with Figures 9 and 12, we conclude that inclusion of the azimuthal variation in power pattern results in poorer agreement between theory and experiment for the boresight pointing accuracy.

3.4 Diffuse Multipath Power

The boresight error includes a diffuse multipath contribution and, for completeness, that result is also presented. Figure 13 shows the variation in P_{DIFF} for the same parameter values used in the case of Figure 12. Comparison of Figure 13 with Figure 8 shows that the diffuse multipath power in the difference channel is between 30 dB to 50 dB less than the coherent power in the sum channel.

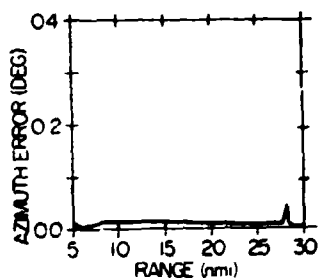


Figure 12. Theoretical Calculations: σ_θ vs Range, $k_m = 1.5$, Shadowing, Exponential PDF, Azimuthal Pattern Variation

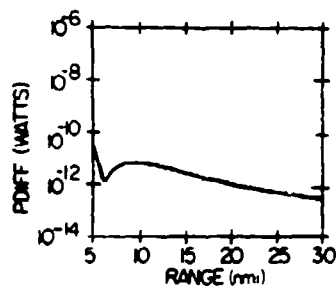


Figure 13. Theoretical Calculations: Diffuse Power (P_{DIFF}) vs Range, $k_m = 1.5$, Shadowing, Exponential PDF, Azimuthal Pattern Variation

3.5 Conclusion

The results of this report are being extended. Improved techniques for the estimation of statistical parameters characterizing the terrain and alternative methods for hypothesis testing of the PDF of the terrain heights are being pursued. Further improvements involve the introduction of mean surface tilt effects, models that contain two scales of surface roughness, and the azimuthal variations of the normalized rough surface cross section, σ_o . Preliminary results indicate that inclusion of the azimuthal variation of σ_o results in excellent agreement between theory and experiment for boresight pointing error.

References

1. Beckmann, P., and Spizzichino, A. (1963) The Scattering of Electromagnetic Waves From Rough Surfaces, Macmillan Co.
2. Ruck, G. T., Barrick, D. E., Stuart, W. D., and Krichbaum, C. K. (1970) Radar Cross Section Handbook, Vol. 2, Plenum Press.
3. Long, M. W. (1975) Radar Reflectivity of Land and Sea, Lexington Books.
4. Brown, G. S. (1978) Backscattering from a Gaussian-distributed perfectly conducting rough surface, IEEE Trans. on Antennas and Prop. AP-25(No. 3):472.
5. Whalen, A. D. (1971) Detection of Signals in Noise, Academic Press.
6. Hagfors, T. (1964) Backscattering from an undulating surface with applications to radar returns from the moon, J. Geophys. Res. 69:3779.
7. Barrick, D. E. (1968) Relationship between slope probability density function and the physical optics integral in rough surface scattering, Proc. IEEE 56:1728.
8. Semenov, B. I. (1965) Scattering of electromagnetic waves from restricted portions of rough surfaces with finite conductivity, Radiotekh. i Elektron 10:1952.
9. Sancer, M. I. (1969) Shadow-corrected Electromagnetic scattering from a randomly rough surface, IEEE Trans. on Antennas and Prop. AP-17:577-585.
10. Brown, G. S. (1980) Shadowing by non-Gaussian random surfaces, Proceedings of the Second Workshop on Terrain and Sea Scatter, George Washington University, Washington, D. C.
11. McGarty, T. P. (1975) The Statistical Characteristics of Diffuse Multipath and its Effect on Antenna Performance, AD-A009869.
12. Mood, A. M., and Graybill, F. A. (1963) Introduction to the Theory of Statistics, McGraw-Hill.
13. Jenkins, G. M., and Watts, D. G. (1968) Spectral Analysis and its Applications, Holden-Day.
14. Lennon, J. F., and Papa, R. J. (1980) Statistical Characterization of Rough Terrain, RADC-TR-80-9, RADC/EE Hanscom AFB, Massachusetts.
15. Lytle, R. J. (1974) Measurement of earth medium electrical characteristics: Techniques, Results and Applications, IEEE Trans. on Geoscience Electronics, GE-12:81.
16. Peake, W. H. (1959) The Interaction of Electromagnetic Waves With Some Natural Surfaces, Antenna Laboratory, Ohio State University, Report No. 898-2.
17. Wright, J. W. (1968) A new model for sea clutter, IEEE Trans. on Antennas and Prop. AP-16:217-223.
18. Fuks, I. (1966) Contribution to the theory of radio wave scattering on the perturbed sea surface, Iz. Vyssh. Ucheb. Zaved. Radiofiz., 5:876.
19. Barton, D. K., and Ward, H. R. (1969) Handbook of Radar Measurement, Prentice-Hall.
20. Abramowitz, M., and Stegun, I. A. (1968) Handbook of Mathematical Functions, U.S. Govt. Printing Office.

Appendix A

The Shadowing Function for Exponentially Distributed Surface Heights

Brown¹⁰ has derived an explicit expression for the shadowing function in the case of backscatter when the bivariate PDF for the surface slopes has an exponential form. Here, we present the corresponding results for bistatic scattering, based on Brown's work. In conformity with Eq. (20) in Section 4.1, let the polar angles of incidence and scattering be denoted by θ_i and θ_s , and let the azimuthal angles of incidence and scattering be denoted by ϕ_i and ϕ_s . Also, let S_{exp} denote the shadowing function when the bivariate PDF for the surface slopes is exponentially distributed. Then, for the special case when $\phi_s = \pi + \theta_i$:

$$S_{\text{exp}} = \frac{1}{C_0 + 1} \text{ for } \theta_s \leq \theta_i$$

and

$$S_{\text{exp}} = \frac{1}{C_2 + 1} \text{ for } \theta_s \geq \theta_i.$$

For all other cases:

$$S_{\text{exp}} = \frac{1}{C_0 + C_2 + 1}.$$

For normally distributed surface heights, the expressions for C_0 and C_2 are given by Sancer.⁹ Here, for exponentially distributed surface slopes, the expressions for C_0 and C_2 are given by

$$C_0 = (x_1/\pi) K_2(x_1) - 1/2 + (x_1/2) [K_1(x_1)L_0(x_1) + L_1(x_1)K_0(x_1)]$$

and

$$C_2 = (x_s/\pi) K_2(x_s) - 1/2 + (x_s/2) [K_1(x_s)L_0(x_s) + L_1(x_s)K_0(x_s)]$$

where

$$x_1 = [\sqrt{6} / (2\sigma/T)] \cot \theta_1 ,$$

$$x_s = [\sqrt{6} / (2\sigma/T)] \cot \theta_s ,$$

$K_i(x)$ = Modified Bessel function of the second kind of order i ,

and

$L_j(x)$ = Modified Struve function of order j (see Reference 20) .

20. Abramowitz, M., and Stegun, I. A. (1968) Handbook of Mathematical Functions, U.S. Govt. Printing Office.

Appendix B

Specular Region Characterization

The purpose of this discussion is to describe the region contributing to the coherent multipath at the receiving antenna. For the case of interest, the angles of incidence are relatively small. The approximation is made that only the first Fresnel zone effect is significant; successive phase differences between the remaining zones produce terms that would destructively interfere with each other at the receiver.

The Fresnel zones can be described by a family of nested ellipses. The curves in Figure 3 show the range dependence of the zone length, width, center point, and specular point location. These results are based on relations found in Beckmann and Spizzichino.¹

The results are given in terms of target distance L from the receiving antenna along the ground projection of the target trajectory. L_1 is the distance to the specular point, h_A is the antenna height above sea level, h_T the transmitter height, and \bar{z}_{sp} the mean height of the subregion containing the specular point. First,

$$L_1 = \left[\frac{(h_A - \bar{z}_{sp}) L}{(h_a - \bar{z}_{sp}) + (h_T - \bar{z}_{sp})} \right] \quad (\text{m}).$$

To establish the Fresnel zone length and width, we define the path length distance relative to the direct ray, δ_0 , as

$$\delta_o = \frac{2(h_A - \bar{z}_{sp})(h_T - \bar{z}_{sp})}{L} \text{ (m)}$$

where

δ_o , h_A , and h_T are all much smaller than L .

Then, the center of the elliptical zone X_{01} is given by

$$X_{01} = \left(\frac{L}{2} \right) \left[\frac{\lambda L + 2(h_A - \bar{z}_{sp})(h_A + h_T - 2\bar{z}_{sp})}{\lambda L + (h_A + h_T - 2\bar{z}_{sp})^2} \right] \text{ (km)},$$

the semimajor axis intercept, X_{11} is given by

$$X_{11} = \left(\frac{\sqrt{\lambda} L^2}{2} \right) \left[\frac{(\lambda + 2\delta_o)^{1/2}}{\lambda L + (h_A + h_T - 2\bar{z}_{sp})^2} \right] \text{ (km)},$$

and the semiminor axis intercept, Y_{11} is given by

$$Y_{11} = \left(\frac{\sqrt{\lambda} L^2}{2} \right) \left[\frac{\lambda + 2\delta_o}{\lambda L + (h_A + h_T - 2\bar{z}_{sp})^2} \right]^{1/2} \text{ (m)}.$$

It should be noted that these expressions are approximate ones and that there is considerable discussion as to just what is the actual region that contributes to the specular multipath.

Appendix C

The Azimuthal Variation of the Monopulse Difference Pattern

In order to obtain a more realistic value for the azimuthal power pattern contribution to the power at the monopulse receiving antenna, the original simple constant value was replaced by values based on the actual difference (power) pattern described by McGarty.¹¹ This azimuthal monopulse difference pattern is illustrated in Figure C1.

For our purpose, the intensity (y-axis of the figure) was converted from dB into pure numbers (that is, -10 dB = 0.1, -20 dB = 0.01, and so on. The main null in the difference pattern was assumed to have a value of $y = 0$ at azimuth angle, $x = 0.0^\circ$ (x-axis of the figure). The two peaks in the difference pattern that occur at $x = \pm 2.5^\circ$ are assumed to have an intensity $y = -4 \text{ dB} = 0.398$. Since the average sidelobe level is less than or equal to $-45 \text{ dB} = 0.0000316$, the intensity at $x \geq 5.0^\circ$ was set equal to $y = 0$.

We approximated half the difference pattern (y values for $x \geq 0$) by fitting a parabola through the three points ($x = 0^\circ$, $y = 0$), ($x = 2.5^\circ$, $y = 0.398$) and ($x = 5^\circ$, $y = 0.0$). This parabola is represented by the equation:

$$y = -0.0637 x^2 + 0.3184 x .$$

We want to determine the relation of the half width of the glistening surface, l_{GS} as defined by Beckmann and Spizzichino,¹ to the half width of the antenna pattern footprint on the ground l_{FP} . Let R_{FP} be the range from the monopulse antenna to the point on the ground and recall that $x_{FP} = 5^\circ$ on the difference pattern, the value beyond which the intensity $y = 0$. Then

$$l_{FP} = R_{FP} \tan x_{FP} = R_{FP} \tan 5^\circ ,$$

$$l_{GS} = R_{FP} \tan x_{GS} .$$

In the computer program for calculating the coherent and incoherent power reaching the monopulse receiving antenna, the total receiving antenna power pattern is taken to be the triple product of the azimuthal pattern given by Figure C1 (difference pattern) multiplied by the elevation power pattern (difference pattern, given in the report by McGarty)¹¹ multiplied by the sum channel gain (32.5 dB). In this Appendix, we are considering the effects only of the azimuthal power pattern—the elevation power pattern and sum channel gain have been normalized to unity in the present form of the expression. Then, the average power P_{AV} , from the glistening surface detected in the difference channel is

$$P_{AV} = \left(\frac{1}{2 x_{GS}} \right) (2) \int_0^{x_{GS}} y(x) dx$$

or

$$P_{AV} = -0.02123 x_{GS}^2 + 0.159 x_{GS} \quad \text{for } l_{GS} \leq l_{FP}$$

and

$$P_{AV} = -0.02123 x_{FP}^2 + 0.159 x_{FP} \quad \text{for } l_{GS} \geq l_{FP}$$

Note that in the last expression the contributions to the diffuse power from points of the glistening surface beyond l_{FP} are considered negligible because of the low antenna side lobes.

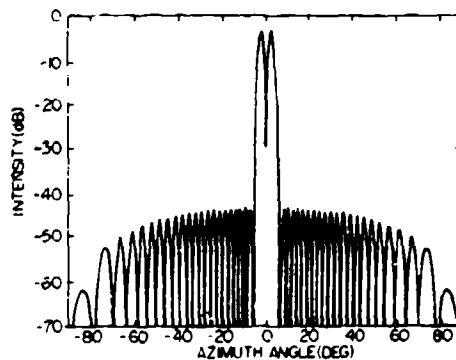


Figure C1. Monopulse Difference Pattern in Azimuthal Plane